# SLAM performance prediction using CNNs

Matteo Princisgh

*I declare that this material, which I now submit for assessment, is entirely my own work and has not been taken from the work of others, save and to the extent that such work has been cited and acknowledged within the text of my work. I understand that plagiarism, collusion, and copying are grave and serious offences in the university and accept the penalties that would be imposed should I engage in plagiarism, collusion or copying. This assignment, or any part of it, has not been previously submitted by me or any other person for assessment on this or any other course of study.*

## 1 Introduction

In the field of autonomous mobile robotics, there are many tasks that a robot has to perform in order to explore a new environment. One of these tasks is Simultaneous Localization And Mapping (SLAM), which is a well-known chicken-and-egg problem, where an accurate estimate of a robot pose is needed to create an accurate map, and vice versa an accurate map is needed to effectively estimate its pose.

### 1.1 Related work

In the last decades, with the development of many new SLAM algorithms and techniques, there has been a growing need to find a common evaluation metric/framework. Many solutions are based either on manual evaluation [1], or on other external information about the environment and robot operation. For example, a widely used metric that requires the latter is the Absolute Pose Error (APE), proposed by Kümmerle et al. in [2], which is divided into two sub-metrics: the Absolute Translational Error (ATE) and the Absolute Rotational Error (ARE). **Figure 1** shows how the ATE varies during the exploration of an environment, but for this work the main focus is on the average value calculated after the environment has been fully explored.

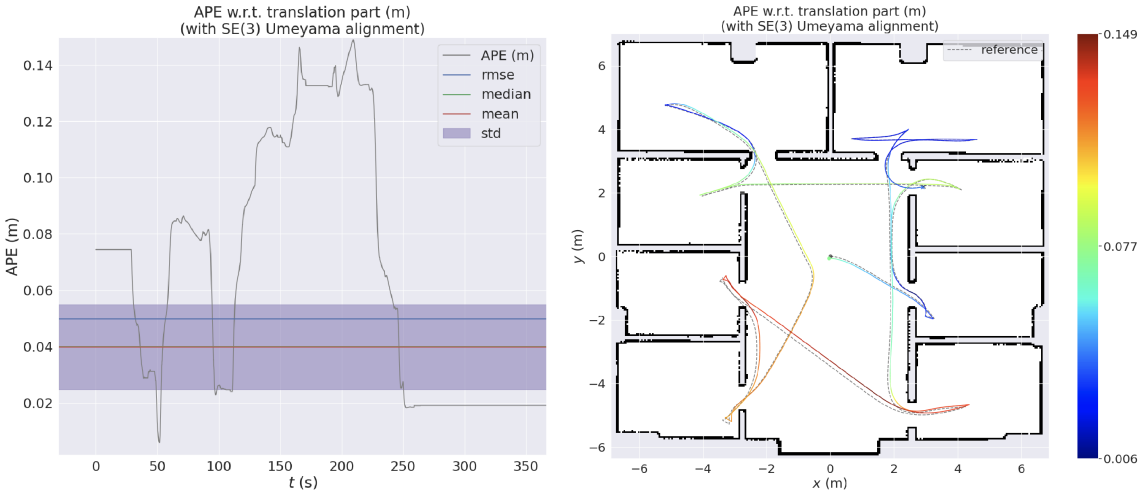


**(a)** ATE variation over time

**(b)** ATE values over the map

**Figure 1:** Visualizations of ATE variations during exploration, realized with *evo*[1].

[1]https://github.com/MichaelGrupp/evo

In order to compute ATE and ARE values after a robot has explored an environment, we need to compare all the pairs of key-points sampled from the estimated trajectory of the robot and its ground truth (GT) trajectory. Specifically, during exploration we sample $T$ poses, where each pose is a vector containing the position and orientation of the robot, and we build two sets $x_{1:T}$, $x^*_{1:T}$ that contain, respectively, the estimated and GT poses.
Next, we define $\delta_{i,j} = x_j \ominus x_i$ as the relative transformation[2] that moves the robot from pose $x_i$ to $x_j$, and its counterpart $\delta^*_{i,j} = x^*_j \ominus x^*_j$. Then we define the $trans(\cdot)$ and $rot(\cdot)$ functions which extract, respectively, the translational component of a transform (i.e., a vector $z_{ij} \in \mathbb{R}^2$ representing the translation delta needed to move from pose i to j) and the rotational component (i.e., a vector $\theta_{ij} \in \mathbb{R}^2$ that expresses the angular deltas as Euler angles). Finally, to compute the localization error we consider all sorted pairs of transformations $\{\delta_{i,j} : j < i, \forall i \in 2 \dots T\}$:

$$
\begin{aligned}
\varepsilon(\delta) &= \varepsilon_t(\delta) + \varepsilon_r(\delta) \\
&= \frac{1}{N} \sum_{i,j} trans(\delta_{i,j} \ominus \delta^*_{i,j}) + \frac{1}{N} \sum_{i,j} rot(\delta_{i,j} \ominus \delta^*_{i,j}) \\
&= \frac{1}{N} \sum_{i,j} (||z_{ij} - z^*_{ij}||_2 + ||\theta_{ij} - \theta^*_{ij}||_2) \\
&= \frac{2}{(T-1)^2} \sum_{i=2}^{T} \sum_{j=1}^{i-1} (||z_{ij} - z^*_{ij}||_2 + ||\theta_{ij} - \theta^*_{ij}||_2)
\end{aligned}
$$

Note that these metrics are dependent on the availability of the GT data, which is easily obtained in simulated environments but extremely difficult to obtain when deploying a robot in the real world, as it would require an external system for accurately tracking its real position.

To address the limitation of depending on the GT data, Luperto et al. in [3], propose a method to perform an *a-priori* prediction of the expected ATE and ARE, based on the geometric/topological characteristics of an indoor environment: using a feature extractor, described by Luperto et al. in [4], a set of structural features is extracted from a floorplan, in order to represent each environment as a vector $v \in \mathbb{R}^k$, where $k$ is the number of distinct features. Successively, each environment is explored by a simulated robot and, by collecting both GT and estimated trajectories, the corresponding ATE and ARE are computed and stored.
Finally, two models are trained on this dataset:

- **Linear model:** computed using linear regression.
- **Gaussian Process:** computed using an RBF kernel.

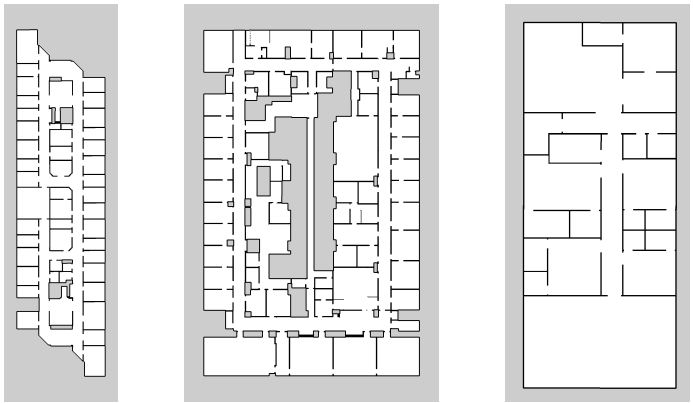

**(a)** KTH **(b)** MIT **(c)** HouseExpo

**Figure 2:** Example of floorplans from the datasets used in this work.

[2]Which is a transformation matrix that describes a rigid transform.

### 1.2 Task formulation

The goal of this project is to evaluate how a predictor, based on state-of-the-art convolutional neural networks (CNN), performs with respect to the aforementioned models. In particular, with the usage of a CNN, it is possible to delegate the feature extraction stage to the network itself, so that a floorplan's image can be fed directly to the model, without computing a set of hand-crafted features.
The dataset used in this work was collected for my Bachelor's thesis *'Structural analysis of indoor environments for improving autonomous robotic tasks'*, and consists of floorplans and exploration data from three different sources: MIT campus [5], KTH campus [6], and HouseExpo [7]. The joint dataset consists of 5933 floorplans, and contains both domestic and work/school environments, as shown in **Fig 2**.

Each floorplan has associated three quantities: area ($m^2$), ATE ($m$), and ARE ($rad$); the floorplan image, together with the area, forms the input, while the labels consist of tuples containing the ATE and ARE values.
More formally, the model $h$ we want to learn can be expressed as follows:

$$h : X \to Y \ , \ X \in (Mat_{n \times n} \times \mathbb{R}), \ Y \in \mathbb{R}^2$$

## 2 Data preprocessing

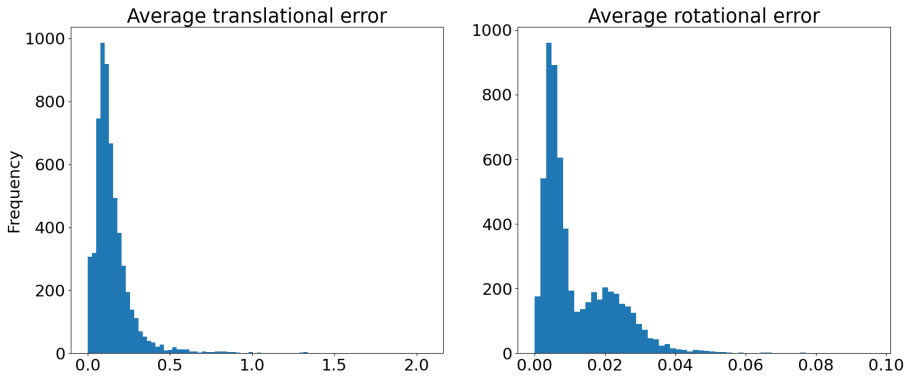


**Figure 3:** Original localization error distribution

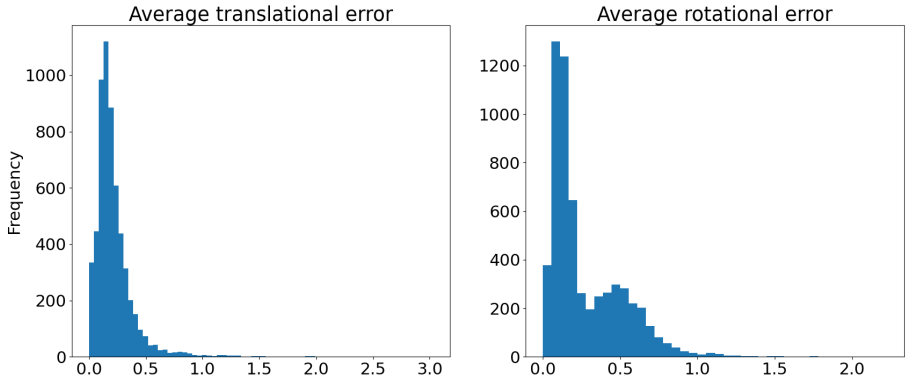


**Figure 4:** Re-scaled localization errors

Both the ATE and ARE distributions exhibit right skewness, with the presence of a few outliers (Figure 3). To mitigate the effects of vanishing gradients and the influence of outliers, the data is scaled so that 99% of the values fall between 0 and 1, as shown in Figure 4. Additionally, the area of each floorplan is normalized to the $[0, 1]$ range by dividing each datapoint by the maximum area value in the dataset.

### 2.1 Image loading and dataset creation

Another preprocessing step consists in fixing images' resolution so that they can be fed to the CNN: for each floorplan we compute the minimum circumscribed square and scale it to a size [3] of 500x500px. Floorplan images are loaded and processed lazily using TensorFlow's `data` API[4], which handles automatically the allocation and de-allocation policies for the images.

After splitting the floorplans in the usual train/validation/test partitions, respectively with 70/15/15 thresholds, the dataset creation steps consist of:

1. Image loading.
2. Data augmentation, which randomly rotates an image by multiples of 90°.
3. Creation of each datapoint tuple `(image, area, label)`.
4. Shuffling and batching of datapoints into mini-batches of size 64.

Note that the data augmentation step is applied at runtime only on the training set, in order to improve the model generalization capabilities.

## 3 Model architecture

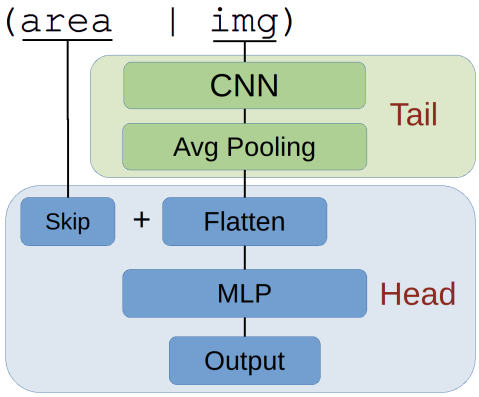


**Figure 5:** High level overview of the model structure.

The model can be divided in two distinct sections: a *tail* CNN, responsible for feature extraction, and a *head*, which is a multilayer perceptron (MLP), that produces the output, as shown in **Fig 5**.

The fact that the `area` input is connected to the MLP is due to the image scaling step described in section 2.1: the original floorplans are represented in a specific resolution, for which it is known exactly how many pixels in the image represent a meter in the real building, but after rescaling the image to a fixed resolution this information is lost.
A robot exploring two environments of different sizes but identical layouts would yield different localization errors, while the model would produce the same output since the scaled input images are identical. Intuitively, an average localization error of $1m$ assumes a radically different meaning if an environment is very small (worse case) or very big.
Thus, the skip connection for the area parameter, which in practice becomes a bias term, is needed to compensate for the lost information about the environment size.

All the experiments described in the following sections have been repeated with three different tail CNNs: ResNet [8], EfficientNetV2 [9] and MobileNetV3 [10]. Considering that a hypothetical deployment of this model to a robotic platform would incur in several hardware limitations, by repeating the experiments it is possible to empirically assess the performance/inference time trade-off of using one architecture over the other with respect to this specific task.

[3] This resolution choice is rather generous, given that both CNNs internally re-scale the image to 224x224px. Storing the dataset at a higher resolution leaves some margin for future experiments with different models.

[4] https://www.tensorflow.org/guide/data

### 3.1 Residual networks

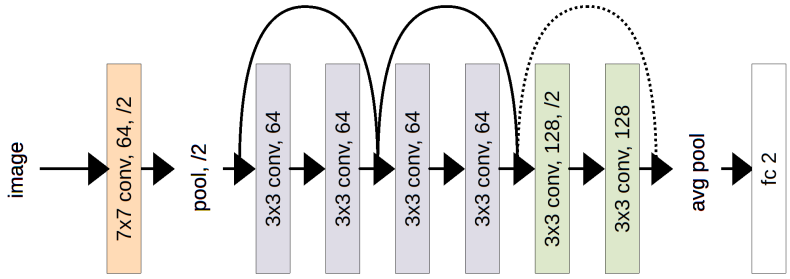


**Figure 6:** Layer configuration of the custom ResNet.

The ResNet network used in this work was implemented from scratch, and its layers are summarized in **Fig 6**. The main characteristic of this architecture is the usage of shortcut connections, represented by the curved lines, which propagates the input matrix of two (or more) stacked blocks and sums it elment-wise to their output (before the activation function). In case the first stacked block reduces the size of its input, the shortcut adjusts the matrix size by performing 1x1 convolutions with a stride of 2 (the dashed shortcut). The usage of these skip connections mitigates the training accuracy degradation phenomenon, where deeper networks converge to a training error higher than shallower ones, indicating that, as the depth of a CNN increases over a certain threshold, the optimizers are not capable of finding better solutions (i.e., it becomes easier getting stuck in a local minima).
The stacked blocks (i.e., the colored tiles in **Fig 6**) consist of the following layers:

- **Convolutional layer**, which learns a set of filters (64, 128, or 256) using kernels of size 3x3, except from the first stacked block, which uses a 7x7 kernel. In order to reduce the size of the input tensors, some layers use a stride of two (i.e., the '/2' field in the blocks).
- **Batch Normalization** [11], which normalizes the output of the convolutional layer in order to have zero mean and unit variance, and then applies an additional translation and scaling using two learned parameters $\gamma$ and $\beta$:

$$\hat{x}_i = \frac{x_i - \mu_{\mathcal{B}}}{\sqrt{\sigma^2_{\mathcal{B}} + \epsilon}}$$
$$y_i = \gamma \hat{x}_i + \beta$$

  Where $x_i$ is the output of the convolutional layer, $\mu_{\mathcal{B}}$ and $\sigma^2_{\mathcal{B}}$ are the sample mean and sample variance of the elements of mini-batch $\mathcal{B}$, and $\epsilon$ is an arbitrarily small constant needed for numerical stability.

- **Activation layer**: which simply computes the non-linear activation function over the output of the previous layers, in this instance the $ReLU$ function: $y_i = max(0, x_i)$.

Additionally, the max pooling layer used before the residual blocks, down-samples the feature maps of the preceding convolutional layer; it does so by taking the maximum activation value in a 2x2 kernel passed over each feature map with a stride of two.

The EfficientNet and MobileNet architectures are based on residual networks and explore different layer combinations and scaling techniques aimed at reducing inference time and number of parameters, while improving the accuracy of the network. The EfficientNet and MobileNet weights used in this work were pre-trained on the *imagenet* dataset [12] and are kept frozen in the following stages; thus, only the MLP weights are adjusted during training.

Instead, the ResNet weights are trained on our dataset, in order to compare its performance versus that of a CNN trained on a generic classification task (i.e., on *imagenet*). Training a CNN from scratch is a data-hungry process, depending on the network size, but given the fact that the maps used in this work are visually simple and relatively noise-free, a shallow CNN would probably be capable of extracting the features needed for our task. Thus, even with a small training set of around 4000 images, it should still be feasible to train a network capable of competing with more

complex architectures.

Finally, the hidden layers of the MLP, as well as the output layer, use ReLU as the activation function, and the choice on using any regularization technique, such as Batch Normalization or Dropout, is delegated to the hyperparameter selection phase.

# 4 Hyperparameter selection

In order to find the *best-performing* model, there were two possible choices for hyperparameter (HP) optimization:

- Perform a random search, over a small HP space, while using $k$-fold cross-validation on each combination of values.
- Perform black-box optimization over a larger HP search space, but test each combination only on the validation set (due to time constraints).

Ultimately, the choice fell on the latter option and the Optuna [13] framework was used to perform black-box optimization. Given the size of the dataset and the training step time of the models, each training run required a time ranging from 5 up to 20 minutes (on a machine with an RTX2080). This meant that choosing the second HP optimization approach allows for testing a much larger set of HP values for a fixed time budget; specifically, for a given $k$ value of folds in the first approach in the same time frame we would be able to test only $\frac{1}{k}$ HP configurations. The trade-off of the second approach is an increase of uncertainty in the estimation of the model's performance of each HP configuration.

## 4.1 Sampling and pruning algorithms

The two main components used in the optimization phase are Tree-structured Parzen Estimators (TPE) [14], which belongs to the family of Bayesian optimization algorithms for generating new HPs, and HyperBand [15] for pruning trials with poorly-performing HPs.
The TPE sampler works as follows:

1. Take as input the hyperparameter search space $\mathcal{H}$.
2. Perform $n$ startup trials (in our case $n = 10$) by randomly sampling sets of parameters $p \in \mathcal{H}$, and score each trial according to the validation loss produced by the model built with $p$.
3. Divide the trials in two partitions, using a quantile $\gamma$ for thresholding, and define two distributions; the 'good' distribution $\ell(t)$ and the 'bad' distribution $\mathrm{g}(t)$, created using a Gaussian Mixture Estimator over the two partitions.
4. To find the next best set $p^*$, we draw $k$ samples distributed according to $\ell(t)$, and build the candidate set $S := \{p_i \sim \ell(t),\ \forall i = 1 \dots k\}$. Then we extract $p^*$ as follows:

$$p^* = \arg\max_{p \in S} \frac{\mathbb{P}(p \in \ell(t))}{\mathbb{P}(p \in \mathrm{g}(t))}$$

   Meaning that we want to extract a $p^*$ that maximizes the likelihood of belonging to the 'good' distribution, while minimizing the probability that it belongs to the 'bad' one.

Steps 3 and 4 are repeated each time a new set of HPs is drawn and evaluated, so that the distribution $\ell(t)$ is updated in order to converge to a region that minimizes the validation loss of the models built by extracting HPs from it.

The HyperBand algorithm is needed to detect and prune trials with poor HP configurations, thus avoiding wasting time and resources on training models with poor hyperparameters. It works by modeling the budget allocation problem as a Multi-Armed Bandit (MAB) problem: each HP configuration is a bandit, and the algorithm tries to find the optimal exploration/exploitation trade-off, where the explorative approach consists in testing many configurations for a short number of

iterations, versus the exploitative approach which tests fewer configurations but with a greater allocation of resources.

Given a finite number of trials $T$, which is the maximum global number of training runs to be performed, HyperBand allocates the trials across a set of brackets and assigns a budget $\beta$ to each bracket. The budget can be either a time limit or a resource limit; the default budget metric for the Optuna implementation is the number of training epochs.
The example in **Table 1** is useful to intuitively understand how the algorithm works: there are $k = 3$ brackets, in which the leftmost is the explorative one and the rightmost is the exploitative one; the $n_i$ field indicates the number of HP configurations that are to be tested during the $i$-th iteration, and $b_i$ is the budget allocated to each configuration, where $b_i = \frac{\beta}{n_i}$.

| Brackets | | | | | | |
|---|---|---|---|---|---|---|
| $i$ | $n_i$ | $b_i$ | $n_i$ | $b_i$ | $n_i$ | $b_i$ |
| 0 | 16 | 1 | 4 | 4 | 2 | 8 |
| 1 | 8 | 2 | 2 | 8 | 1 | 16 |
| 2 | 4 | 4 | 1 | 16 | - | - |
| 3 | 2 | 8 | - | - | - | - |
| 4 | 1 | 16 | - | - | - | - |

**Table 1:** Example of budget allocation of HyperBand.

At the end of each iteration $i$, the worst performing configurations are discarded and the better ones are trained in the subsequent iteration with additional budget. In the example, the number of configurations kept for the successive iteration is $\frac{n_i}{2}$, but a different fractional coefficient $\eta$ can be chosen to reduce the number of iterations. Finally, each bracket requires $\lfloor \log_\eta(n_0) \rfloor$ trials to be completed, which means that the example above would require 41 trials to test 22 different HP combinations, spending a total budget of 160 epochs.

The stopping criterion for each HP optimization step, other than HyperBand pruning, is EarlyStopping with a patience of 7 epochs with respect to the validation loss. Finally, the limit of optimization runs (i.e., the *Trial* parameter in **Algorithm 1**) is set to 50, the minimum resource allocated to each trial is three epochs and the maximum is 20.

The optimization process can be summarized as follows:

**Algorithm 1:** Optimize Hyperparameters

```
sampler ← TPE();
p ← baseline parameters;
v* ← ∞;
for i ∈ 1...Trials do
    m ← train_model(p) ;          // stop training with pruning or EarlyStopping
    v ← evaluate_model(m);                          // compute the validation loss
    if v < v* then
        v* ← v;
        p* ← p
    end
    p ← sampler.Sample();
end
return p*;                                    // return HPs that minimize val loss
```

## 4.2 Optimized architectures

One of the advantages of using the Optuna framework is the possibility of visualizing the relative importance of each HP involved in the optimization process, as well as the contour plot of the objective value with respect to the variation of pairs of parameters, as shown in **Figure 7**. These visualizations give some insight on how the various combinations of HP affect the model performance and may be useful in case of an eventual ablation study.

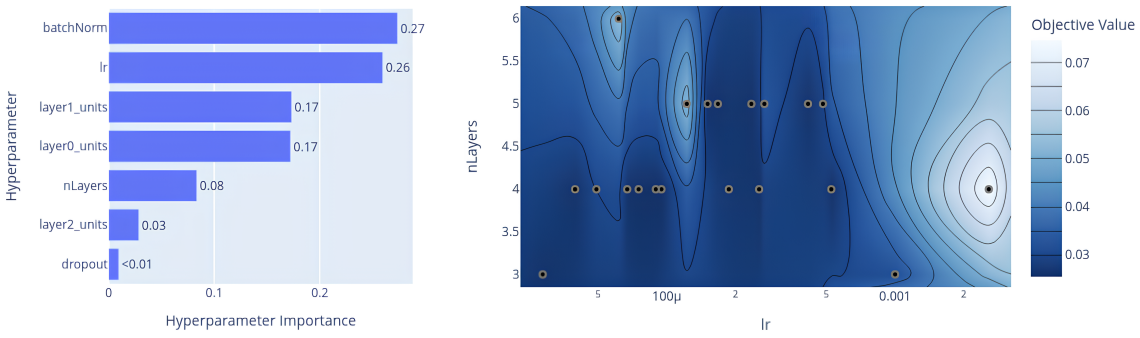


**Figure 7:** Relative importance and contour plot of the validation loss variation with respect to learning rate and number of MLP layers.

The list of tunable HPs, as well as their optimal values, is shown in **Table 2**, where we observe how the optimization process converged to some peculiar combinations of layers for the MLP head: for example, the EfficientNet head consists of five layers with [256, 256, 1024, 512, 512] units, which is a fairly unusual succession of layers. Moreover, for all architectures apart from ResNet, neither batch normalization nor dropout were used, which leads to models that converge very quickly to good validation losses, but tend to overfit for longer training runs, as described in the next section.

| | **Baseline** | **ResNet** | **EfficientNet** | **MobileNet** |
|---|---|---|---|---|
| Learning Rate | 1$e$-4 | 2e-4 | 5$e$-4 | 1.3$e$-3 |
| Batch Norm. | Yes | No | No | No |
| Dropout | No | Yes | No | No |
| Dense layers | 3 | 1 | 5 | 5 |
| Units per layer | [1024, 512, 128] | [1024] | [256, 256, 1024, 512, 512] | [512, 64, 64, 64, 128] |

**Table 2:** Manually selected HP (baseline) vs optimized HP.

# 5 Training the models

In order to train our custom ResNet CNN, the SGD optimizer was used with mostly the same HPs as the original paper, minus the learning rate, which is two orders of magnitude smaller due to the fact that our network is shallower than the original one. The loss function is MSE, and the SGD HPs used for training are:

- **Learning rate:** $\eta = 1 \times 10^{-3}$, with a plateau decaying factor of 0.2, meaning that if during training the validation loss becomes stationary, the LR is reduced to allow for finer gradient steps necessary for converging to a local minima.
- **Momentum:** $\beta = 0.9$, which applies gradient smoothing using a weighted moving average on the succession of gradients. Formally:

$$m_t = \beta m_{t-1} + (1-\beta)\nabla L(W_t)$$
$$W_{t+1} = W_t - \eta_t m_t$$

  Where $m_t$ is the gradient computed at time $t$, $W_t$ are the weights of the network, $\nabla L$ is the loss gradient (computed wrt. a random extraction of one datapoint), $\eta_t$ is the learning rate, and $\beta$ is the momentum.
- **Weight Decay:** $\lambda = 1 \times 10^{-4}$, is a regularization technique which consists in adding to the loss a penalty term proportional to the L2 norm of the weights in the network.
  Putting it all together, the penalty term and final weight update become:

$$L_\lambda(W) = L(W) + \frac{\lambda}{2}||W||^2$$
$$W_{t+1} = W_t - \eta_t(m_t + \lambda W_t)$$

Apart from the ResNet training, all subsequent training runs have been performed using the *Adam* [16] optimizer and MSE as the loss function.

*Adam* combines the momentum technique described above, with *RMSProp*, which is a similar technique but considers the weighted moving average of the squared gradients, which approximates the gradients variance:

$$V_t = \gamma V_{t-1} + (1-\gamma)(\nabla L(W_t, X_t, Y_t))^2$$

Then uses the squared root of this moving average to adaptively reduce the learning rate. Thus, the update rule for the weights becomes:

$$W_t = W_{t-1} - \frac{\eta_t m_t}{\sqrt{V_t + \epsilon}}$$

This ensures that each weight of the network is adjusted adaptively, with momentum smoothing and scaled updates in case of large gradients[5]. The stopping criterion for each run was EarlyStopping, with a patience of 7 epochs, and after stopping the training process, the best weights (i.e., those that minimize validation loss) are restored and saved to disk.

## 5.1 Training results

After having optimized each model, a training run is performed with the best HPs and $k$-fold cross validation is used to obtain robust estimates for the model performances. The results are summarized in **Table 3**, whereas **Figure 8** shows the training loss and validation loss curves observed during training.

| Model | Train Loss | Val Loss | Test Loss | 5-fold CV |
|---|---|---|---|---|
| **ResNet** | | | | |
| Baseline | 0.0368 | 0.0365 | 0.0354 | 0.0416 |
| Optimized | 0.0366 | **0.0358** | **0.0352** | **0.0367** |
| **EfficientNet** | | | | |
| Baseline | 0.0355 | 0.0370 | 0.0364 | 0.0382 |
| Optimized | 0.0351 | 0.0361 | 0.0363 | 0.0376 |
| **MobileNet** | | | | |
| Baseline | 0.0261 | 0.0417 | 0.0452 | 0.0471 |
| Optimized | 0.0359 | 0.0362 | 0.0356 | 0.0519 |

**Table 3:** Baseline vs optimized performance of the three CNNs.

Finally, the number of parameters and the inference time of the optimized models are summarized in **Table 4**, where the GPU used for these tests is an RTX2080 and the CPU an i7-9700K. The inference times reported are relative to a single datapoint; calculated by dividing the inference time of a batch by its cardinality.

| Model | Tail params | Head params | t-GPU(ms) | t-CPU(ms) |
|---|---|---|---|---|
| **ResNet** | 389˙760 | 135˙170 | 0.6 | 4.2 |
| **EfficientNet** | 12˙930˙622 | 1˙511˙170 | 15.2 | 562 |
| **MobileNet** | 2˙996˙352 | 542˙274 | 4.5 | 250 |

**Table 4:** Parameters count and inference time of each optimized model.

[5]The additional bias correction steps for the $m_t$ and $V_t$ terms were omitted for brevity.

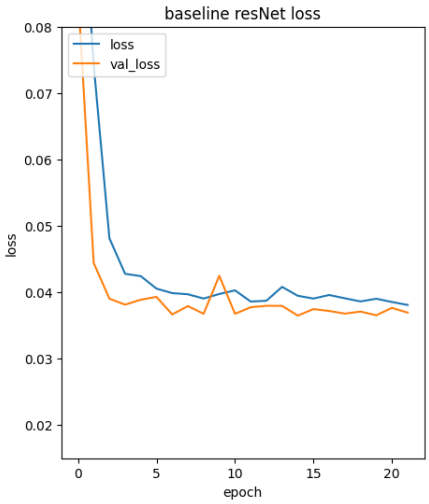


**(a)** Baseline ResNet

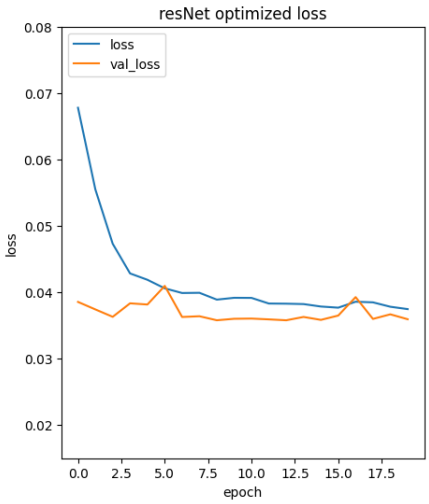


**(b)** Optimized ResNet

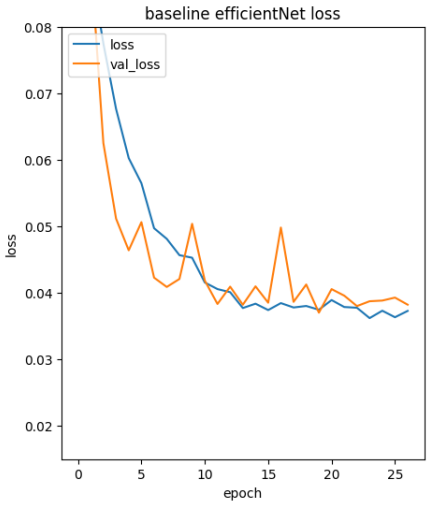


**(c)** Baseline EfficientNet

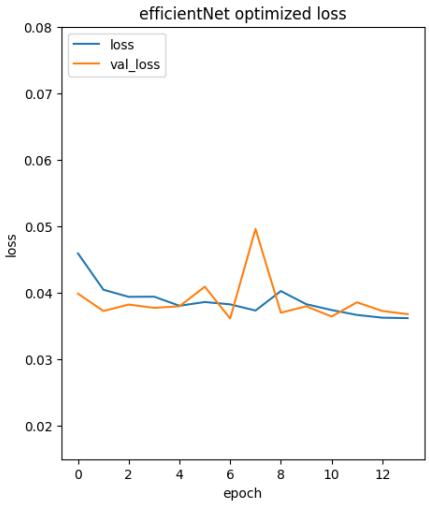


**(d)** Optimized EfficientNet

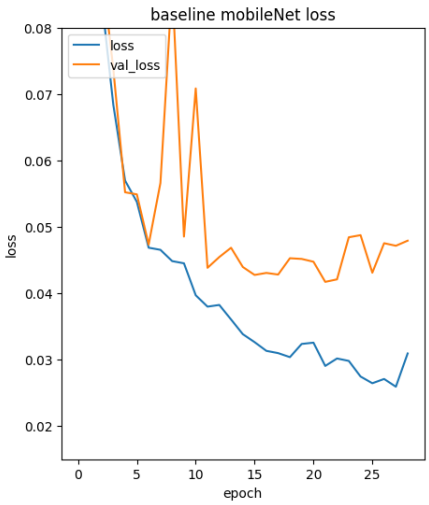


**(e)** Baseline MobileNet

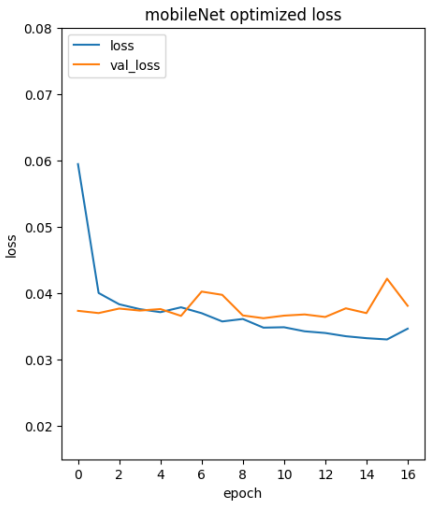


**(f)** Optimized MobileNet

**Figure 8:** Training curves of the various models

# 6 Experimental results

Finally, once the models have been optimized and trained, it is possible to assess their performance relative to the two models described in Section 1.1, using the same metrics as in the article (i.e., R2 score, RMSE, and NRMSE).

As shown in **Table 5**, our custom ResNet performs slightly better than the linear model to predict both translational and rotational error.

| **ATE** | **R2-score** | **RMSE** | **NRMSE** |
|---|---|---|---|
| ResNet | 0.45 | **0.101** | **0.049** |
| EfficientNet | 0.40 | 0.105 | 0.051 |
| MobileNet | 0.39 | 0.106 | 0.052 |
| Linear Model | **0.46** | 0.104 | 0.050 |
| Gaussian Process | 0.27 | 0.104 | 0.050 |
| **ARE** | **R2-score** | **RMSE** | **NRMSE** |
| ResNet | **0.050** | **0.0095** | **0.131** |
| EfficientNet | 0.040 | 0.0096 | 0.132 |
| MobileNet | 0.043 | 0.0096 | 0.132 |
| Linear Model | 0.050 | 0.0099 | 0.136 |
| Gaussian Process | -9.47 | 0.0327 | 0.449 |

**Table 5:** Performance comparison of CNNs vs traditional models.

The fact that the ResNet model performed better than its pre-trained counterparts is likely due to the fact that the CNN was trained specifically on the kind of images that we are working with. This can also be seen by the fact that, after the optimization process, the pre-trained models have deeper, more complex heads, whereas the ResNet model only needs a single layer with 1024 units. Moreover, it achieved the best score during $k$-fold cross validation, meaning that it is very likely the model is capable of generalizing well.

The deployment of the ResNet model on a robotic platform would also benefit from having a very small inference time, which is two orders of magnitude smaller than the next-best CNN model (i.e., EfficientNet).

Further improvements of these results may include:

- Extend the hyperparameter selection phase to perform neural architecture search (NAS) and optimization of the ResNet CNN layers
- Fine-tuning of the pre-trained models
- Usage of other tail architectures, like attention-based models; although the usage of transformers would require a much bigger labeled dataset which is, to the best of my knowledge, not publicly available.

# References


[1] Benjamin Balaguer, Stefano Carpin, and Stephen Balakirsky. Towards quantitative comparisons of robot algorithms: Experiences with slam in simulation and real world systems. In *IROS 2007 workshop*, 2007.

[2] Rainer Kümmerle, Bastian Steder, Christian Dornhege, Michael Ruhnke, Giorgio Grisetti, Cyrill Stachniss, and Alexander Kleiner. On measuring the accuracy of slam algorithms. *Autonomous Robots*, 2009.

[3] Matteo Luperto, Valerio Castelli, Fabio Bonsignorio, Francesco Amigoni, et al. Predicting performance of slam algorithms. In *Artificial Intelligence and Robotics workshop at AI* IA (Italian Association for Artificial Intelligence)*, 2021.

[4] Matteo Luperto and Francesco Amigoni. Extracting structure of buildings using layout reconstruction. In *Intelligent Autonomous Systems 15: Proceedings of the 15th International Conference IAS-15*, 2019.

[5] Emily J Whiting. *Geometric, topological & semantic analysis of multi-building floor plan data.* PhD thesis, Massachusetts Institute of Technology, 2006.

[6] Patric Jensfelt Alper Aydemir and John Folkesson. What can we learn from 38,000 rooms? reasoning about unexplored space in indoor environments. In *2012 IEEE/RSJ International Conference on Intelligent Robots and Systems (IROS)*, 2012.

[7] Li Tingguang, Ho Danny, Li Chenming, Zhu Delong, Wang Chaoqun, and Max Q.-H. Meng. Houseexpo: A large-scale 2d indoor layout dataset for learning-based algorithms on mobile robots. *arXiv preprint arXiv:1903.09845*, 2019.

[8] Kaiming He, Xiangyu Zhang, Shaoqing Ren, and Jian Sun. Deep residual learning for image recognition. In *Proceedings of the IEEE conference on computer vision and pattern recognition*, 2016.

[9] Mingxing Tan and Quoc Le. Efficientnetv2: Smaller models and faster training. In *International conference on machine learning*, 2021.

[10] Andrew Howard, Mark Sandler, Grace Chu, Liang-Chieh Chen, Bo Chen, Mingxing Tan, Weijun Wang, Yukun Zhu, Ruoming Pang, Vijay Vasudevan, et al. Searching for mobilenetv3. In *Proceedings of the IEEE/CVF international conference on computer vision*, 2019.

[11] Sergey Ioffe. Batch normalization: Accelerating deep network training by reducing internal covariate shift. *arXiv preprint arXiv:1502.03167*, 2015.

[12] Jia Deng, Wei Dong, Richard Socher, Li-Jia Li, Kai Li, and Li Fei-Fei. Imagenet: A large-scale hierarchical image database. In *2009 IEEE conference on computer vision and pattern recognition*, 2009.

[13] Takuya Akiba, Shotaro Sano, Toshihiko Yanase, Takeru Ohta, and Masanori Koyama. Optuna: A next-generation hyperparameter optimization framework. In *Proceedings of the 25th ACM SIGKDD international conference on knowledge discovery & data mining*, 2019.

[14] James Bergstra, Rémi Bardenet, Yoshua Bengio, and Balázs Kégl. Algorithms for hyper-parameter optimization. *Advances in neural information processing systems*, 2011.

[15] Lisha Li, Kevin Jamieson, Giulia DeSalvo, Afshin Rostamizadeh, and Ameet Talwalkar. Hyperband: A novel bandit-based approach to hyperparameter optimization. *Journal of Machine Learning Research*, 2018.

[16] Diederik P Kingma. Adam: A method for stochastic optimization. *arXiv preprint arXiv:1412.6980*, 2014.